



Depositional modeling of the hydrogenous evaporite salts from the Mediterranean and the Red Sea waters

Nader Ahmed Ahmed Edress¹ · Farida Mohammed Saad El-Din El-Dars²

Received: 25 December 2022 / Accepted: 4 January 2023 / Published online: 16 January 2023
© The Author(s), under exclusive licence to Springer Nature Switzerland AG 2023

Abstract

Changes in seawater chemistry, amounts and ordering of salts precipitated under a closed isotherm evaporation conditions of (45 °C) were probed in the present study to simulate the depositional modeling of salts sequence in nature under similar circumstances. The seawater samples were collected from two shorelines in the territory of Egypt facing the M.S. (Mediterranean Sea) and R.S. (Red Sea). The results reveal that during the process of evaporation (from 0 to 80% water loss), the investigated seawater chemistry exhibits an increase in TDS (total dissolved solids), salinity, density, and (EC) electric conductivity leading to the formation of MgSO₄-enriched seawater brine. As well, the measured pH decreased from 8.9 to 7.57 (M.S.) and from 8.13 to 7.37 (R.S.) toward the formation of a semi-neutral aqueous medium. XRD analysis exhibits the aragonite (CaCO₃) was first to precipitate out from both marine waters at ≤ 20% of the water evaporated, while more soluble halite (NaCl) precipitates from the brine at approximately 75% or even > 80% of the water evaporated. The total amounts of salts precipitated from a 1 L of M.S. and R.S. water were 47.85 g/L and 53.68 g/L, respectively. The average rate of evaporation was 16.63 mL/day and 14.0 mL/day, which was inversely proportional to the induced seawater salinity (M.S. = 31%) and (R.S. = 34.5%). Ultimately, the percentage of salts obtained from 1 L of M.S and R.S water was 21.46 cm³ and 24.62 cm³, respectively, which corresponded to a thin lamina of 2.78 cm and 2.91 cm as appeared in the vertical cross-section for the respective seawater.

Keywords Evaporation sequence · Salt volumes · Arid environments · Mediterranean and Red seawaters · Messinian salinity crisis

Introduction

Evaporites are a type of chemically deposited sedimentary rock. They also mentioned a type of hydrogenous deposits formed when dissolved salts are precipitated via evaporation and concentration of anions and cations in any natural saline aqueous medium (Hardie 1991; Robert 2009; Tucker and Jones 2022). According to Babel and Schreiber (2014), evaporation is a process that brings the under-saturated solution into the state of saturation and supersaturation that

promoting the precipitation of salts from a more saturated one. The efficiency or rate of this process depends upon many factors of temperature (both the brine and ambient), humidity, air movement, and salinity. Other natural geological factors affecting the precipitate of salts within hypersaline basins may include isolated tectonic, eustatic, and climatic change (Khalil et al. 2021; Elhossainy et al. 2022). Nonetheless, evaporite minerals have an important role as palaeo-climate indicators, they are restricted to form under a specific hot climate and arid regions of low latitude, where temperatures are considerably high and the rate of evaporation exceeds the rate of precipitation (rainfall) (Tucker 2001; Nash and McLaren 2011; Nichols 2022).

Accordingly, present-day arid and hyper-arid climate zones extending across North Africa of a great Sahara desert provide favorable conditions to precipitate evaporite salts in an aquatic body of saline water which may occur as perennial saline water lakes and/or closed coastal lagoons. The hyper-arid zones and arid zones of these regions are

✉ Nader Ahmed Ahmed Edress
nedress@outlook.com; nedress@sciences.helwan.edu.eg
Farida Mohammed Saad El-Din El-Dars
fkeldars@hotmail.com; fkeldars@aucegypt.edu

¹ Geology Department, Faculty of Science, Helwan University, Cairo, Egypt

² Chemistry Department, Faculty of Science, Helwan University, Cairo, Egypt

characterized by precipitation (P)/evapotranspiration (ET) ratios ranging between 0.03 and 0.20 (Einsele 2000; Tucker 2001; Leeder 2011; Talebmorad et al. 2021).

The present study aims first to provide a general depositional model from a geological point of view of the precipitated evaporite salts that are deposited from an isolated seawater body by progress evaporation in a hot environmental condition like that occurs in arid climate regions.

The second aim focuses on making the simplest guide for any geologist to calculate and/or estimate several of the primary basic evaporites characteristics concerning: (a) the depositional sequence of evaporites minerals in nature; (b) estimating the rate of evaporation; (c) the role of salinity and density and their effect on the salt-type precipitate; (d) types of salt precipitate and its relation to stages of progress evaporation.

Additionally, the authors shed light on the prediction of a quantity of salt precipitate from the seawater and its thickness that should appear in the ancient geological cross-section. Moreover, the present study modeling applies to understanding the depositional of a huge

evaporate sequence in the Red Sea and the Mediterranean Sea regions during the Messenian Salinity Crisis (MSC) of the Miocene age.

Materials and methods

Sampling

Eight 25-L jerry cans of seawater were collected off the coastal shores of El-Alamein and El-Quseer cities at the Mediterranean and the Red Seas, respectively (Fig. 1). Samples were collected 10–15 m away from the shorelines to ensure that a representative sample was taken from each sea. The samples were transferred to the lab and were sieved through 100 mesh (150 μm) to eliminate any detrital silt, sediments or floating algae, planktons, and aquatic plant remains in preparation for isothermal evaporation procedures.

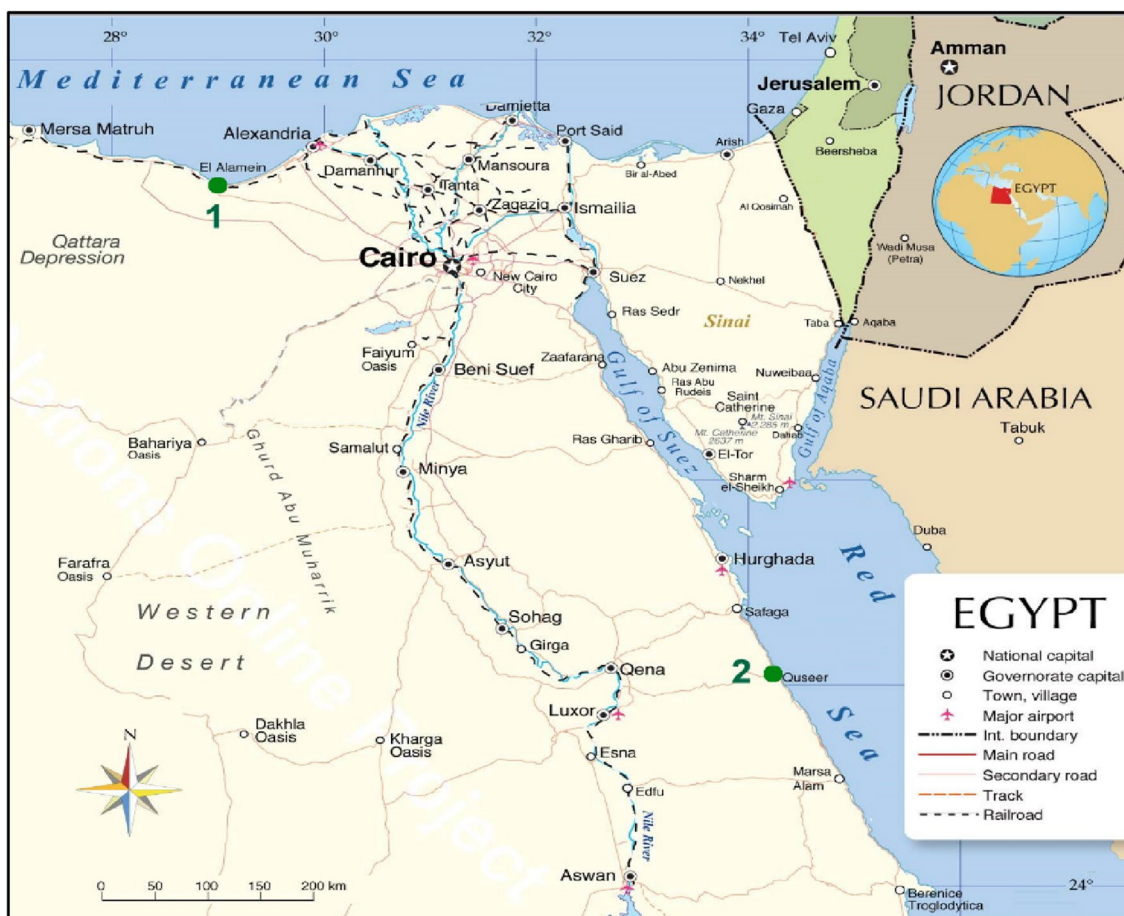


Fig. 1 A map of Egypt showing seawater sampling from the shorelines of El-Alamein city (1) representing the Mediterranean Sea and from the shorelines of El Quseer city (2) representing the Red Sea

Methodology

Figure 2 illustrates the experimental and methodological scheme for both water and salt sampling during the progress of evaporation. Isothermal evaporation experiments were conducted in the lab using two drying ovens each having a capacity of ten 1-L beakers. The temperatures of the ovens were fixed at 45 °C. For each seawater sample, nearly 24 1-L clean and dry beakers were filled to the mark before putting into the oven. The samples were monitored for volume loss at (20, 40, 60, 80, and 100%). At the designated

volume loss, the precipitated (salt crystals) were collected from the solution via filtration using Whatman filter paper (no. 1) and were left to dry at room temperature to a constant weight overnight. The time of evaporation at each volume loss was expressed in days and the mathematical average rate of evaporation was statistically determined. The ionic content (Na^+ , K^+ , Ca^{2+} , Mg^{2+} , CO_3^{2-} , HCO_3^- , Cl^- , SO_4^{2-}) (mg/L), total dissolved solids (TDS) (mg/L), salinity (%), density (g/cm^3), electric conductivity (EC; mS/cm), and pH of the seawater during the progress of the isothermal evaporation were determined analytically by Karl-Fisher Titrator

Fig. 2 A schematic diagram illustrating the experimental and methodological scheme for water–salts sampling and analyses

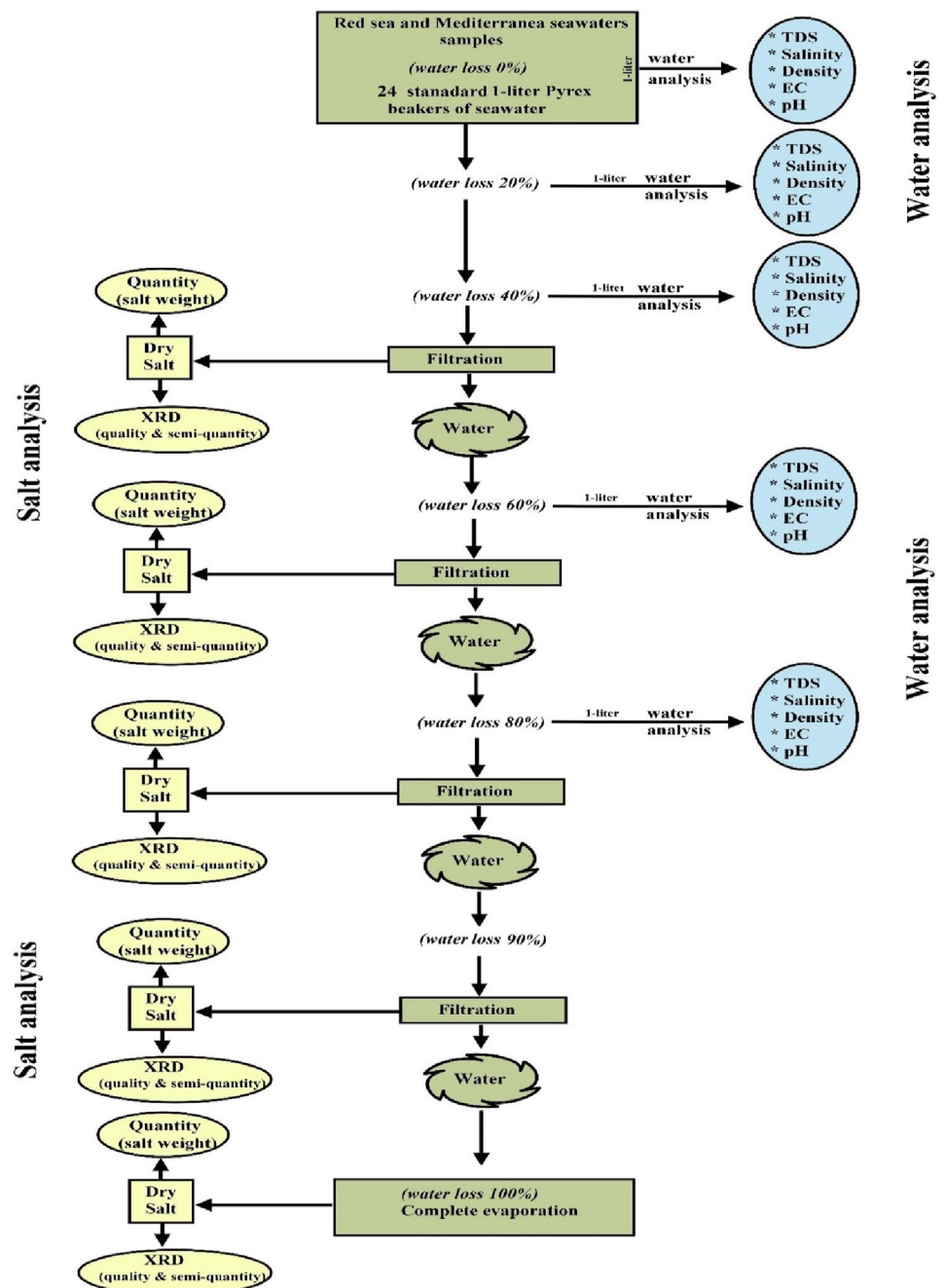


Table 1 Weight of salts precipitated (g/L) from the Mediterranean Sea water during isothermal evaporation

Volume of water Loss parameters	40%	60%	80%	90%	100%
Amounts of water (liter) (Beakers used in each stage)	20	18	15	9	7
Quantity of total filtrated evaporite salts (g)	3.4	29.7	139.8	92.07	185.36
Quantity of evaporite salts per 1 L (g/L)	0.17	1.65	9.32	10.23	26.48
Percentages of salt precipitate in each stage (%)	0.35	3.45	19.48	21.38	55.34
Progress time span (day)	24	38	53	56	64

Table 2 Weight of salts precipitated (g/L) from the Red Sea water during isothermal evaporation

Volume of water loss Parameters	40%	60%	80%	90%	100%
Amounts of water (liter) (Beakers used in each stage)	20	18	15	9	7
Quantity of total filtrated evaporite salts (g)	4	4.86	50.4	115.83	258.86
Quantity of evaporite salts per one liter (g/L)	0.20	0.27	3.36	12.87	36.98
Percentages of salt precipitate in each stage (%)	0.38	0.50	6.26	23.98	68.88
Progress time span (day)	26	41	56	64	71

instrument model (KF-9) at the Central Laboratories of the Egyptian Mineral Resources Authority, Giza, Egypt (Fig. 2).

The filtered salts at each stage of evaporation were left to be completely dry at room temperature for about 2–3 days, and then weighed to determine the amount of the salt precipitated in grams. The types of salt crystals gathered through the various water loss stages of isothermal evaporation were determined using a powder X-ray diffraction instrument. The salt precipitate was analyzed using PANalytical X'Pert Pro MRD, a multipurpose X-ray diffractometer equipped with a Cu K α source. The diffraction charts and relative intensities obtained were compared with ICDD files for the identification of salts, chemical composition, structure, and percentages. X-ray diffraction is carried out at the Central Laboratories of the Egyptian Mineral Resources Authority, Dokki, Egypt.

The time of evaporation per each water loss stage was expressed in days and the average rate of evaporation was statistically determined by Origin Lab Pro Software v.12.

Results

The experimental results concern the chemistry of water samples and the amount of salts precipitated during each stage of the evaporation are summarized in Tables 1, 2, 3, 4 and Figs. 3 and 4. Tables 1 and 2 show the amounts of salts precipitated per 1 L (g/L), percentages of salts precipitate in each stage of evaporation process to reach 100% water, and periods to reach a certain percentage of water loss for both the Mediterranean and Red Sea water. The time to reach 100% of water loss of R.S. was recorded as 71 days notably that takes a long time than that was recorded for M.S. of 64 days for complete dryness.

Tables 3 and 4 provide a detailed counting of the ionic content (Na^+ , K^+ , Ca^{2+} , Mg^{2+} , CO_3^{2-} , HCO_3^- , Cl^- , SO_4^{2-})

(mg/L), TDS (total dissolved solids; mg/L), pH, salinity (%), density (g/cm^3), and EC (electrical conductivity; mS/cm) during each evaporation stages for each analyzed seawater. It is worth noting that for the M.S., the TDS progressively increased to become 4.42 times (189820 mg/L; at 80% water loss) higher than its initial recorded value of 42980 mg/L (at 0% of water loss) (Table 3). The TDS recorded in the R.S. reached (280529 mg/L; at 80% water loss) considered 5.93 times higher than its initial TDS measurement of (47300 mg/L) at 0% water loss. (Table 4). The increase in TDS was accompanied by an increase in salinity, EC, and density. On the other hand, the measured pH showed a trend of decreasing value toward a neutral aqueous medium in both investigated seawaters, as shown in Tables 3 and 4.

Examination of ten salt samples collected (eight by filtration and two after complete dryness) of seawater by XRD techniques shows that the aragonite salt is dominated in stages of 40% and 60% water loss in the case of M.S. and within the stage of 40% water loss in R.S. The threshold precipitation of aragonite salt was recorded in the XRD pattern at the stage of 40–60% of water loss in (M.S.) and at the stage of 40% water loss in (R.S.) (Figs. 3 and 4). The second major evaporite salt recorded in the XRD pattern was gypsum, and its threshold precipitation was recorded at 80% of water loss in M.S. and <80% water loss in R.S. The halite salt recorded with a threshold precipitate peak of 100% water loss in M.S. and at 90–100% water loss in R.S. (Figs. 3 and 4).

The XRD pattern shows an overlap between the precipitations of two evaporate salts of both aragonite and gypsum at 60% water loss in R.S. (Fig. 4). The overlap is also occurring between two other precipitated salts of gypsum and halite at 80% water loss of R.S. (Fig. 4), and the overlap between the same salts of gypsum and halite is shafted toward 90% water loss in case of M.S. (Fig. 3).

Table 3 Variation in the ionic content (Na⁺, K⁺, Ca²⁺, Mg²⁺, CO₃²⁻, HCO₃⁻, Cl⁻, SO₄²⁻) (mg/L), TDS (total dissolved solids; mg/L), pH, salinity (‰), density (g/cm³), and EC (electrical conductivity; mS/cm) for the Mediterranean Sea water during isothermal evaporation

Volume of water loss Parameter	0%	20%	40%	60%	80%
pH	8.90	7.92	7.93	7.72	7.57
Na ⁺ (mg/L)	11,910	15,668	21,853	38,488	57,048
K ⁺ (mg/L)	478	607	860	1461	2147
Ca ²⁺ (mg/L)	476	607	958	1301	1108
Mg ²⁺ (mg/L)	1825	2450	3075	5050	7300
CO ₃ ²⁻ (mg/L)	52.8	14.4	24	33.6	38.4
HCO ₃ ⁻ (mg/L)	4.88	68.3	48.8	43.9	53.7
Cl ⁻ (mg/L)	22,727	30,435	41,998	73,762	107,519
SO ₄ ²⁻ (mg/L)	3300	4230	6140	10,213	12,728
TDS (mg/L)	42,980	55,260	76,280	131,160	189,820
Salinity (%)	31	41.2	59.9	116.1	190.2
Density (g/cm ³)	1.01	1.02	1.03	1.08	1.14
EC (MS/cm)	67.16	86.34	119.19	204.94	297.59

Discussion and conclusions

Ionic contents and development of marine brine type

Warren (2008) distinguished the three major brine types in nature during the evaporation of seawater according to the concentration relationship between Ca²⁺ and HCO₃²⁻ in marine brine next to the precipitation of CaCO₃

Table 4 Variation in the ionic content (Na⁺, K⁺, Ca²⁺, Mg²⁺, CO₃²⁻, HCO₃⁻, Cl⁻, SO₄²⁻) (mg/L), TDS (total dissolve solids; mg/L), pH, salinity (‰), density (g/cm³), and EC (electrical conductivity; mS/cm) for the Red Sea water during isothermal evaporation

Volume% loss Parameter	0%	20%	40%	60%	80%
pH	8.13	8.01	7.89	7.73	7.37
Na ⁺ (mg/L)	13,150	17,208	23,323	33,208	85,718
K ⁺ (mg/L)	508	680	893	1281	3163
Ca ²⁺ (mg/L)	520	656	844	1218	626
Mg ²⁺ (mg/L)	2050	2275	3075	4900	10,550
CO ₃ ²⁻ (mg/L)	38.4	28.8	24	28.8	33.6
HCO ₃ ⁻ (mg/L)	63.4	53.7	63.4	63.4	117
Cl ⁻ (mg/L)	23,856	32,960	43,460	63,661	162,807
SO ₄ ²⁻ (mg/L)	3514	4724	6000	8934	16,925
TDS (mg/L)	47,300	60,080	77,700	113,720	280,520
Salinity (%)	34.5	45.4	61.2	97	340
Density (g/cm ³)	1.02	1.02	1.04	1.06	1.27
EC (MS/cm)	73.91	93.88	121.41	177.69	438.21

(aragonite) to differentiate alkaline Na–K–Mg brine type (HCO₃²⁻ > Ca²⁺) from MgSO₄-enriched and depleted brine types (Ca²⁺ > HCO₃²⁻). Furthermore, he used the Ca²⁺ and SO₄²⁻ concentration for further subdivision of the MgSO₄-enriched seawater (SO₄²⁻ > Ca²⁺) from the MgSO₄-depleted seawater (Ca²⁺ > SO₄²⁻) (Fig. 5). To conclude, the development type of present studied seawaters brine, the concentration of Ca²⁺, HCO₃²⁻, and SO₄²⁻ are counted once after the aragonite precipitation at 60% of seawater loss and second after gypsum precipitate at 80% of seawater loss of both M.S. and R.S. (Figs. 3 and 4). At 60% seawater loss after the precipitation of aragonite, the Ca²⁺ measured as 1301 mg/L (M.S.) and 1218 mg/L (R.S.) showing values much higher than the concentration of HCO₃²⁻ of measured values of 41.9 mg/L (M.S) and 63.4 mg/L (R.S.) (Tables 3 and 4). Where at 80% water loss after the gypsum precipitation, the concentration values of SO₄²⁻ in the brine have a much higher of (12728 mg/L; M.S.) and (16925 mg/L; R.S.) than the concentration of Ca²⁺ of values (1108 mg/L; M.S.) and (626 mg/L; R.S.) toward the formation of the MgSO₄-enriched seawater type (Fig. 5; Tables 3 and 4).

A cross-plot of the main ionic content versus the degree of evaporation of both seawaters concluded that the dominant anions and cations in descending order were Cl⁻ > Na⁺ > SO₄²⁻ > Mg²⁺ > K⁺ ≥ Ca²⁺ > HCO₃⁻ > CO₃²⁻ for both seawaters (Fig. 3a and b). At evaporation stages of 60% to 80%, the Ca²⁺ content exhibited a slight decrease in both brine, which may be due to the consumption of Ca²⁺ by the precipitation of aragonite (CaCO₃) and gypsum (CaSO₄ · 2H₂O) at the earlier stages of evaporation (Fig. 6a and b). Almost dissolved solids gradually increase toward the final stage of complete desiccation. Both the Cl⁻ and Na⁺ show a predominant content in both seawater mediums over any other cations and anion is responsible for the latter precipitation of the halite salt (NaCl) out of both brines in significant amounts.

Salts' precipitation and saline-type stages of seawater

The order of the precipitation of certain evaporite salts from the seawater brine depends essentially upon its solubility. The salt solubility in any aqueous medium is inversely proportional to the salinity and/or density of seawater. Three saline stages were recorded in the present study's evaporation progress. They are mentioned as mesohaline, penesaline-A, and penesaline-B stages. The 40% salinity represents the borderline separating the euhaline (natural seawater) from the mesohaline stage. The mesohaline and penesaline-A stages were separated by the salinity of 140%, while salinity of 250% is marked as the

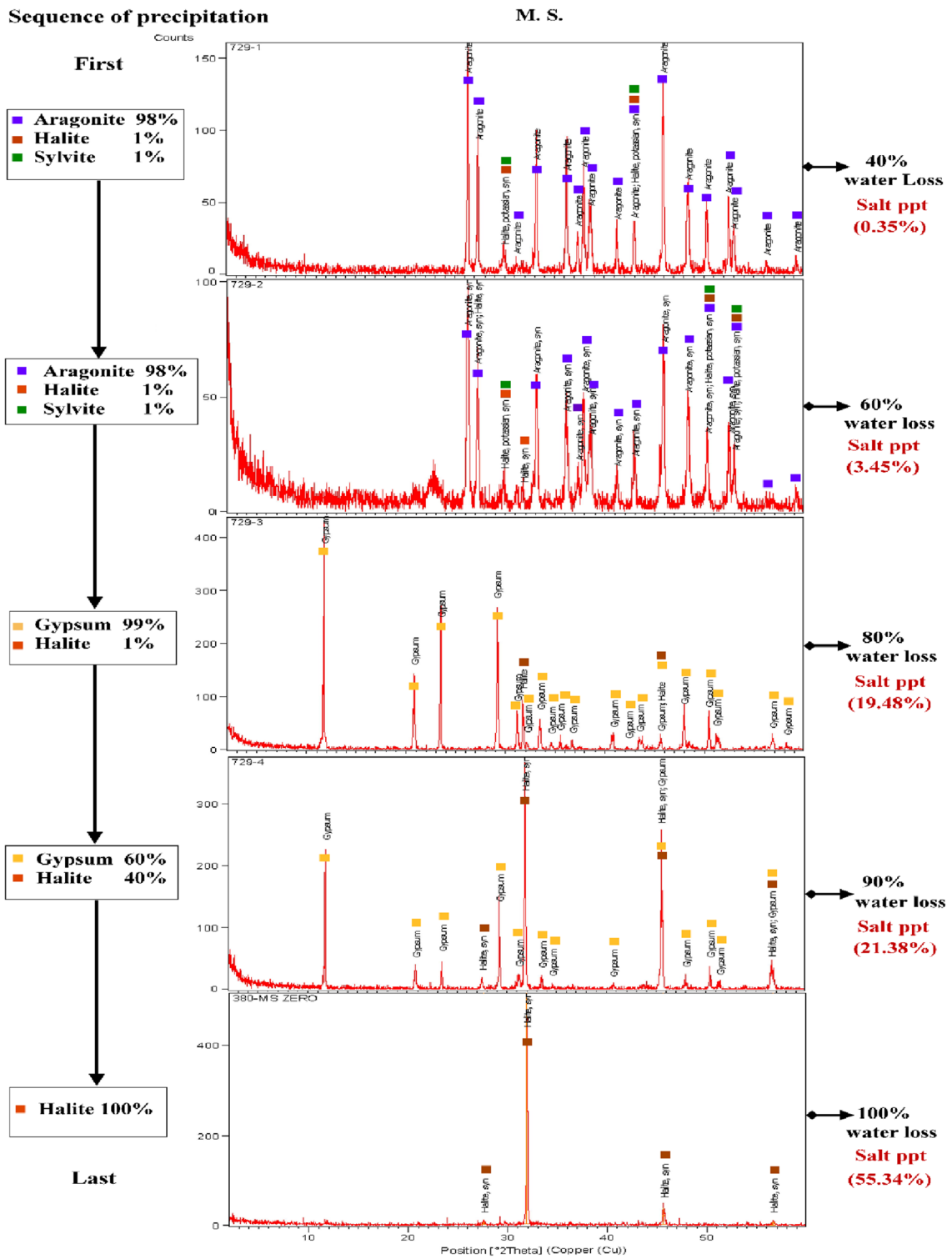


Fig. 3 XRD spectrum of the quantity and quality of evaporate salts precipitate during the various stages of the isothermal evaporation of the Mediterranean Sea water

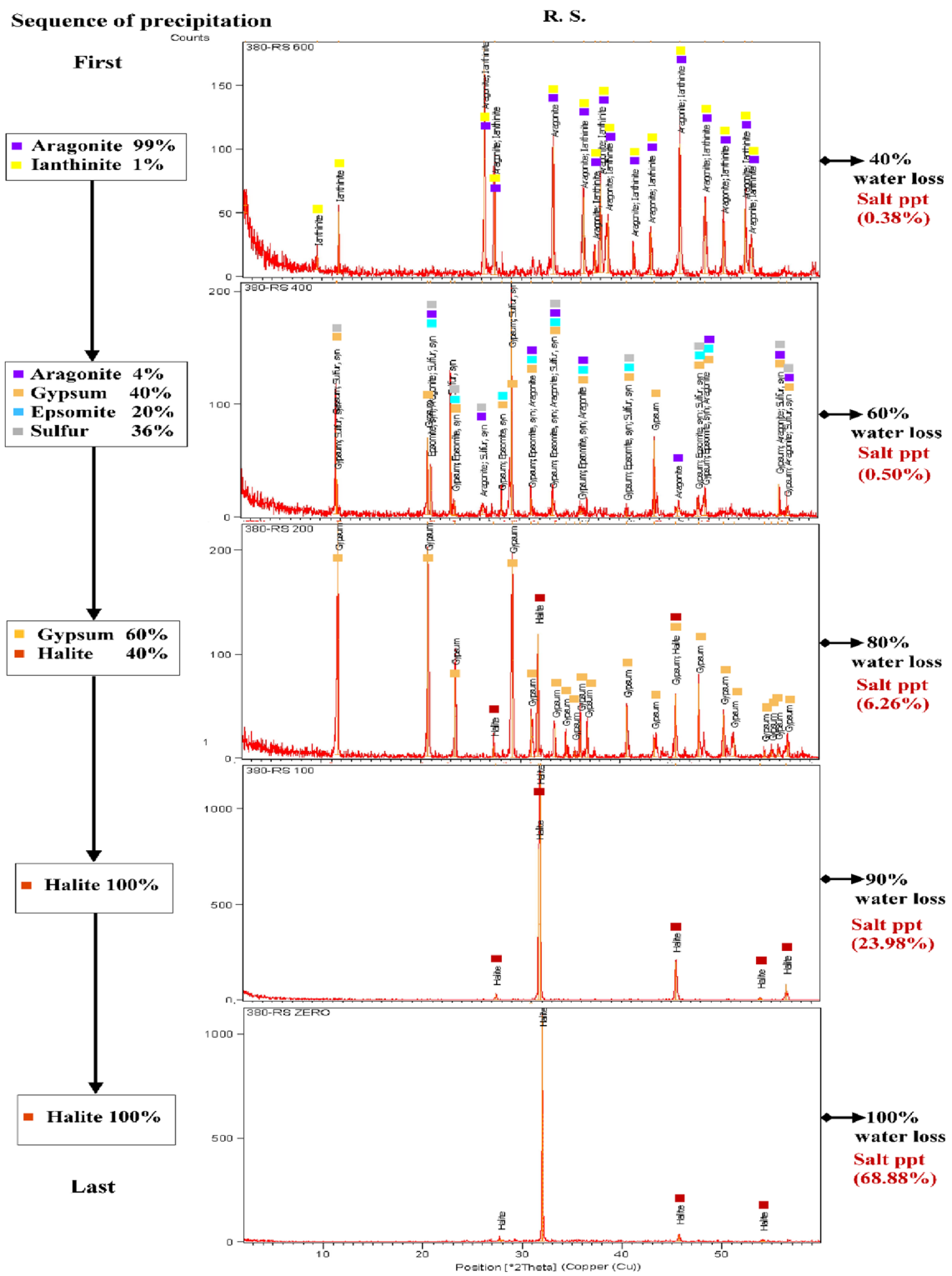


Fig. 4 XRD spectrum of the quantity and quality of evaporate salts precipitate during the various stages of the isothermal evaporation of the Red Sea water

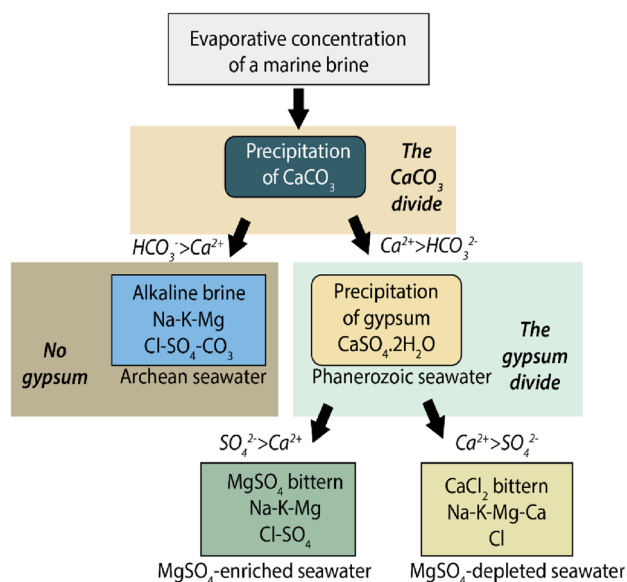


Fig. 5 The sequence of development of the three natural major brine types showing the framework of oceanic chemistry according to Warren (2008)

pensaline-A from the pensaline-B stages (Ostad-Ali-Askari et al. 2017; Warren 2021). The chemistry of each stage promotes the precipitation of certain specified evaporite salts more than the others. Mesohaline is the stage of the precipitation of aragonite salt, pensaline-A is the stage of the precipitation of gypsum salt, and pensaline-B is the stage of the precipitation of halite salt (Fig. 7a and b).

The double plot of TDS versus salinity and density for both the M.S. and R.S. is illustrated in Fig. 7a and b. In the case of M.S. water, the evaporation stages from 20 to 60% lay within the mesohaline stage characterized by the precipitation of aragonite salts, while at 80% of the evaporation process lay within the pensaline-A stage characterized by the precipitation of gypsum salt (Fig. 7a). In case of the R.S. water, the evaporation stages from 20 to 60% lay within the mesohaline stage, characterized by the precipitation of aragonite salts, while at 80% of evaporation process lay within the pensaline-B stage characterized by the precipitation of halite salts. The pensaline-A stage of gypsum salt precipitation is recorded within the evaporation process from higher than 60% to less than 80% of R.S. water (Fig. 7b).

Theoretical estimation and statistical measurement of the evaporation rate

Generally, no equation till the present study was used to estimate the evaporation rate of isolated seawater bodies. The problematic is happen due to the continuously changing in the evaporation rate as a function of changes in the salinity

and density by progressing evaporation. Therefore, the equations used to detect the evaporation rate are restricted to be applied on the isolated freshwater body instead. The present study makes a possibility to estimate the average rate of evaporation of an isolated body of salt brine in nature statistically.

According to Engineering ToolBox (2004), the factors affecting the rate of evaporation from the surface of the freshwater body can be calculated as the following equation:

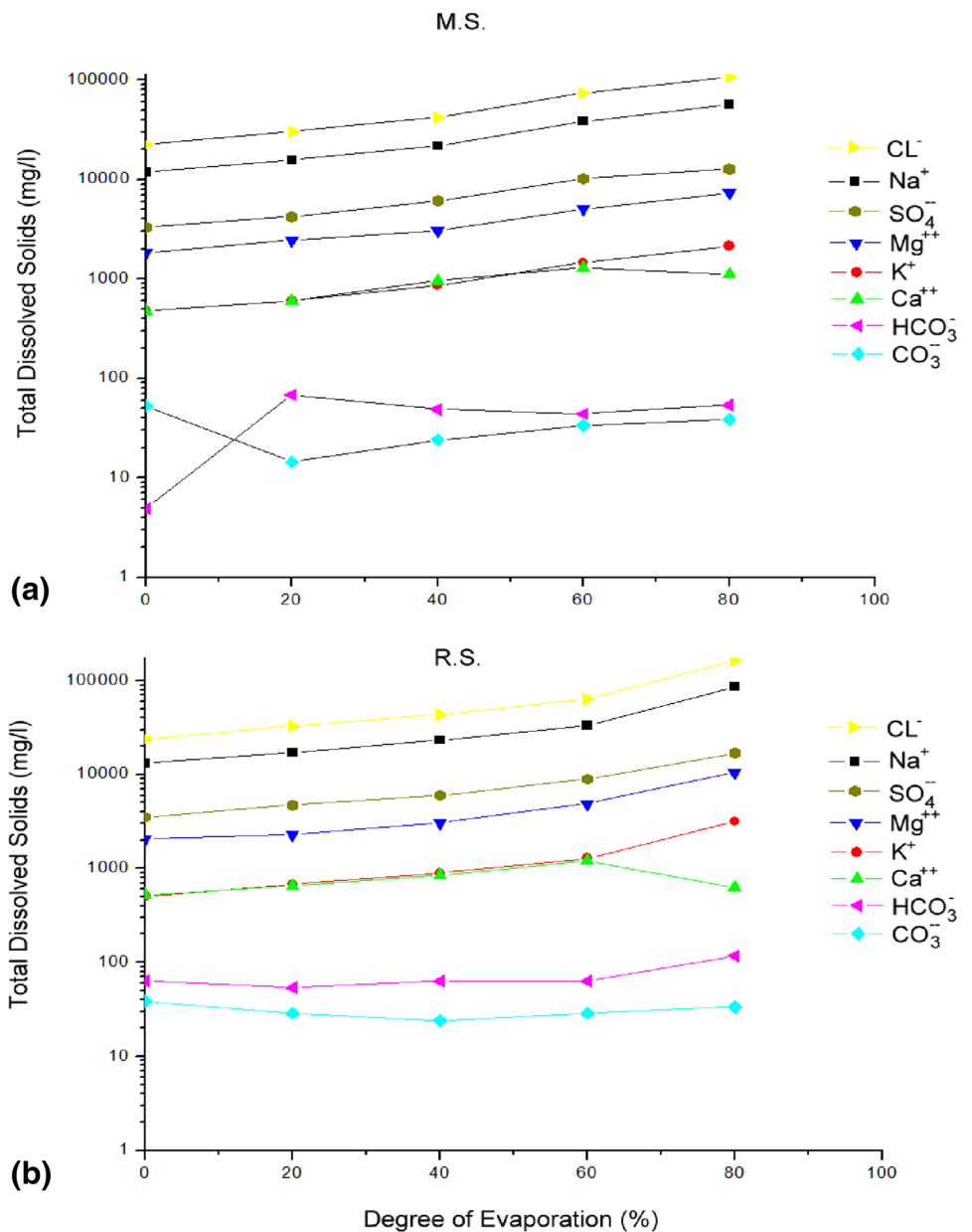
$$gh = \theta A (x_s - x),$$

where gh is the quantity of water evaporated per hour (kg/h), $\theta = (25 + 19v)$ is the coefficient of evaporation (kg/m²h), v is the air velocity above the water surface (m/s), A is the surface area of water (m²), x_s is the ratio of maximum humidity (kg H₂O in kg dry air), and x is the air humidity ratio (kg H₂O in kg dry air).

The above equation was applied for laboratory conditions using the standard water surface area (0.0095 m²) of the beaker surface, air velocity (0), a ratio of maximum humidity (0.054 kg/kg), air humidity ratio (0.033 kg/kg), and the gh amounts of water evaporation per hour = 0.00499 kg/h. The estimated evaporation rate for that volume of standard one beaker of fresh water was calculated as equal to 119.76 mL/day. From which the rate of evaporation for a complete dryness of 1 L of a freshwater beaker in laboratory conditions takes a theoretical 8.35 days. This theoretical calculation of the rate of evaporation coincides with the experimental measurement that was done by the present study by filling 1 L with freshwater and measuring its evaporation rate at a fixed temperature of 45 °C. The complete dryness was taken approximately 9 days. From the above-mentioned conclusion, it appears the applicability of the previous equation to use as a basis for the next statistical steps to determine the average rate of the present study marine waters.

To determine the average rate of evaporation for the studied marine seawater samples, a cross-plot between the degree of evaporation and time of evaporation is presented in Fig. 8 as a statistical polynomial regression. Polynomial regression for 71 reading and 67 reading throughout the experiments had a graphical slope line close to being vertical in the case of the normal stage (euhaline) with an angle of inclination of 64° for M.S. and 45° for R.S. at the initial stage of the evaporation process. This angle shifted to 35° and 28° at the end of the pensaline-B stage of evaporation in respective order (Fig. 10b). Warren (2021) attributed the increase and decrease in the rate of evaporation depending on the change in the chemistry of the saline water medium. He mentioned that the initial stage of hypersaline may exhibit an evaporation rate four times than the normal marine (euhaline), while it increases by 7–11 times in

Fig. 6 Cross log plots of TDS versus the degree of evaporation: **a** for the M.S. water and **b** for the R.S. water



penesaline-A and -B stages and may reach > 11–60 times in the super-saline stage.

From statistical regression diagrams, the initial rate of evaporation for M.S. was 48.53 mL/day, which was decreased to 15.24 mL/day with an average of (15.63 mL/day; 0.00395 kg/h) until reaching complete dryness after 64 days. While the rate of evaporation of R.S. was initiated as 22.75 mL/day and reached 12.73 mL/day with an average of (14.08 mL/day; 0.00356 kg/h).

Other linear statistical strong negative correlation coefficient ($r = -0.99$) is carried out between TDS and gh [quantity of water evaporated per hour (kg/h)] as provided in Fig. 9 for three samples involved points represented a freshwater of TDS equal 500 mg/L, M.S. water of TDS equal

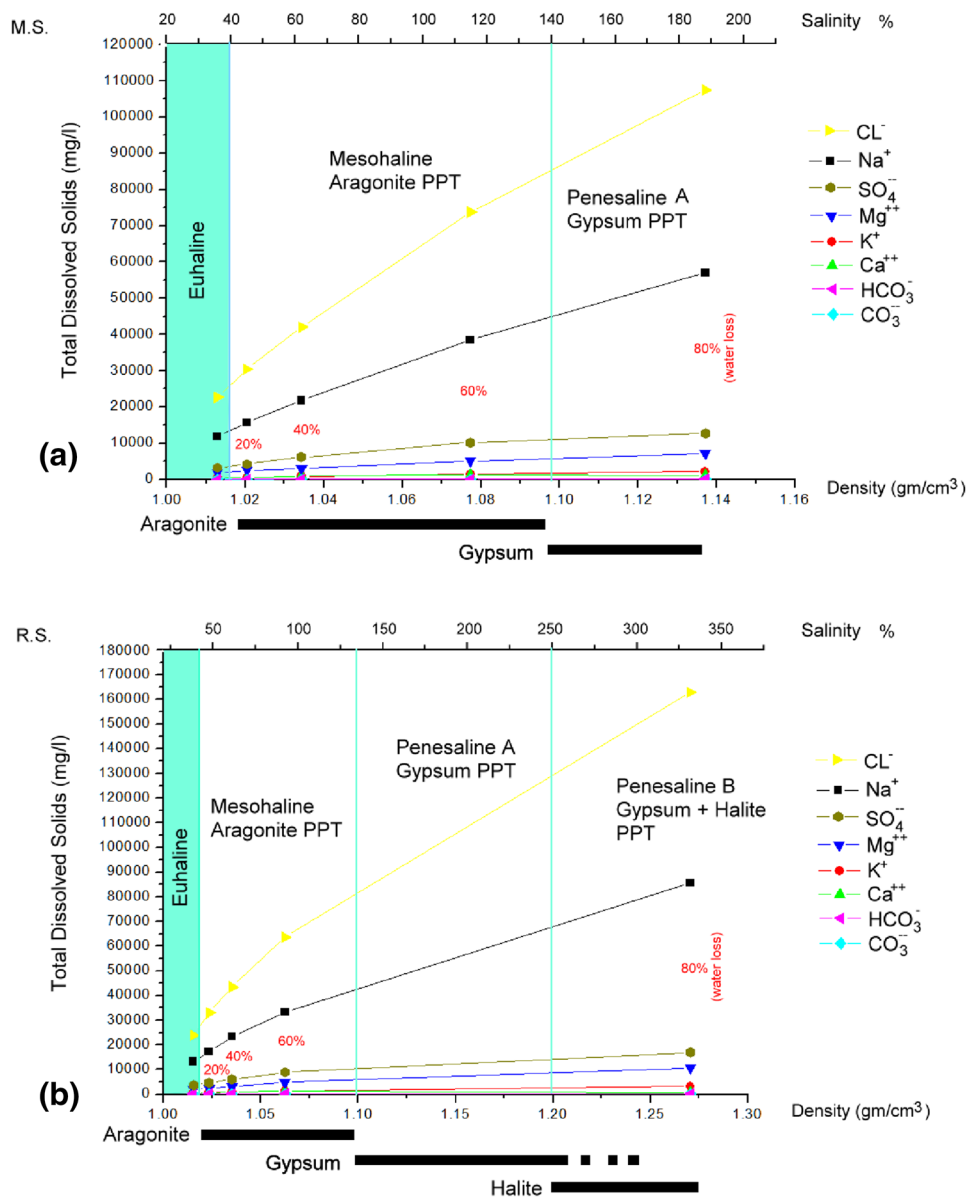
42,980 mg/L, and R.S. water of TDS equal 47300 mg/L. The above-mentioned relationship considers as an attempt by the present study to estimate the average rate of evaporation for an isolated marine water body in nature at a hot-arid climate zone.

Evaporite salts' depositional modeling

Quantitative and qualitative models

The obtained results from the seawater chemistry of collected water samples with the XRD analysis of the precipitate salts collected during the present study evaporation process were merged to give a real illustrated depositional

Fig. 7 Roles of the density and the salinity to distinguish different types of saline stages (mesohaline, penesaline-A, and penesaline-B) of M.S. (a) and R.S. (b) according to Warren (2021)



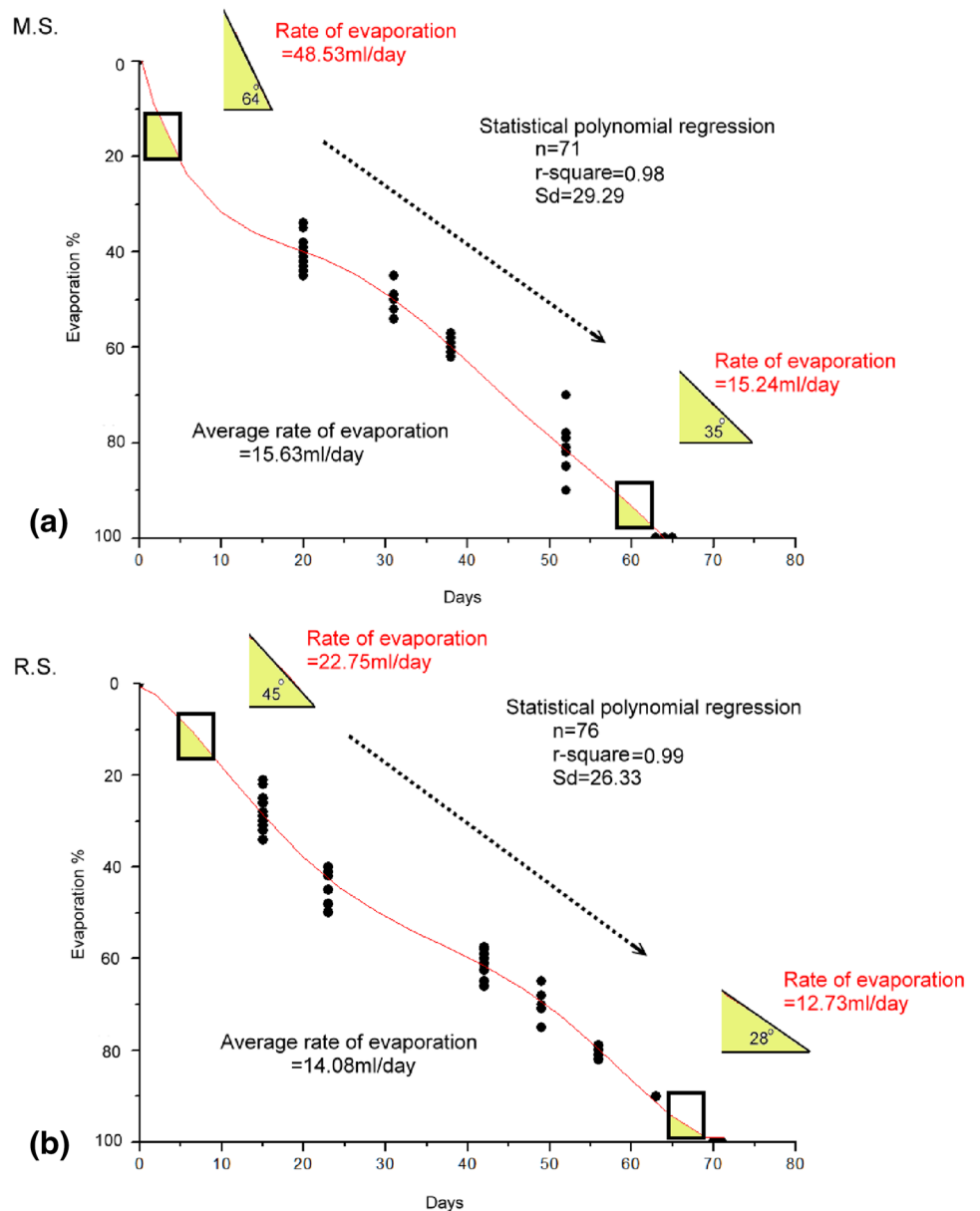
model (Figs. 10 and 11). The modeling shows the quantity and quality of evaporite salts that were precipitated during each stage of the present experiment. Additionally, the author mentioned the favorable deposition condition related to the formation of each evaporite salt from the works of literature to build up a general aspect of salts modeling.

At the 40% volume loss stage, the gain of the evaporite salts was tiny (0.17 g/L) and (0.2 g/L) precipitate in the form of calcium carbonate (CaCO₃) which exists in nature in two forms of orthorhombic and trigonal atomic lattice, namely aragonite and calcite, in which the carbonate ions are packed differently (Borchardt-Ott 2012). Aragonite was favored to precipitate from aqueous solutions more than calcite at elevated temperatures. Nonetheless, Zhong and Mucci (1989) reported in similar experimental procedures

that the precipitation of aragonite was always faster than calcite at 25 °C. As well, they noted that while aragonite was more soluble than calcite, the precipitation of calcite may be preferred if the solution was supersaturated with calcite. While, under-saturated and/or at equilibrium, sea-water medium aragonite preferred to precipitate than calcite.

Sylvite (KCl) and ianthinite (U₄+ (UO₂)₅O₇·10H₂O) were associated with aragonites as an accessory within the 40–60% water loss stage (Figs. 10 and 11). The ianthinite occurrence is very rare in nature (<2%) due to its instability in the presence of oxygen (Singh et al. 2014). As well, knowledge of the stability of ianthinite in natural waters was reported to be limited as it decreased with the increase in temperature. Moreover, ianthinite was reported to be formed under oxygen-deprived atmospheric conditions or

Fig. 8 Statistical polynomial regression between the degree of evaporation and time-consuming until complete dryness: **a** for M.S. water and **b** for R.S. water



in reducing environments at 25 °C and 1 bar of atmospheric pressure (Hazen et al. 2009). As well, they mentioned that most of the uranium enters lakes, inland seas, and oceans with drainage waters, probably delivered as highly soluble uranyl ions or as complex ions containing a uranyl radical, which may explain the occurrence of ianthinite as an accessory mineral in R.S. waters. In the case of the M.S. at 40 and even 60% water loss, sylvite was noted to precipitate with halite at the initial stages. The sylvite mineral intergrown with halite makes a finely granular halite matrix that is referred to as sylvite (Sonnenfeld and Perthuisot 1989). Garrett (1996) reported that sylvite-dissolved halite may be precipitated out of the brine at a temperature range from 39 to 71 °C. As well, it may precipitate out of brines in the presence of NaCl:KCl:MgCl₂ in ratios ranging from 8:1:17

to 1:3.75:17 depending on the temperature of the solute medium.

At the 60% volume loss stage, the number of evaporites deposited was between 0.27 and 1.65 g/L which was equivalent to (0.5–3.45%) for the respective case study seawaters (Tables 1 and 2). Evaporite salts that were precipitated in the Mediterranean seawater at this stage were the same as in the previous stage characterized by the dominance of aragonite with 98% and accessories of sylvite < 1% (Fig. 10). While in the case of Red Seawater, aragonite decreased to be 4% and was replaced by the dominant gypsum (CaSO₄·2H₂O) with 40%, sulfur (S) with 36%, and epsomite (MgSO₄·10H₂O) with 20%. Gypsum (instead of anhydrite) was reported to be the dominant sulfate-precipitated salt at salinities near halite precipitative saturation (Hovorka 1992). With a continuous

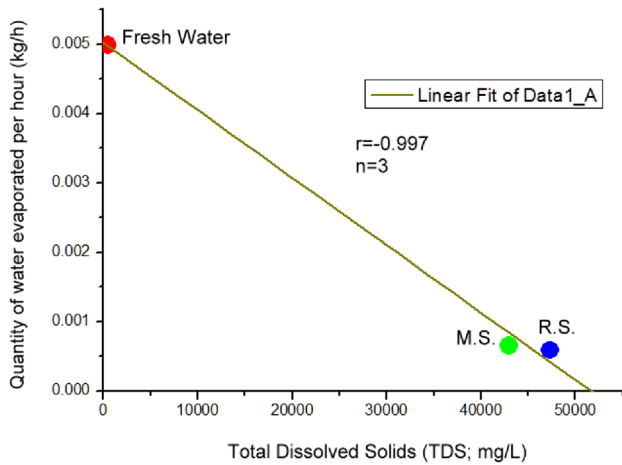


Fig. 9 Linear correlation coefficient relationships between total dissolved solids (TDS; mg/L) and g_h (quantity of water evaporated per hour; kg/h) for fresh and marine seawaters (M.S. and R.S.)

decrease in the volume of the seawater brine, halite extensively replaces the gypsum crystals formed. The source of sulfur and/or sulfide precipitation in the Red Sea brines was reported to be due to the inorganic reduction of sulfate via the mixing of hydrothermal fluids with ambient seawater (Garrett 1996). Sulfate thermochemical reduction caused by hydrocarbons leads to the formation of H_2S and ultimately elemental sulfur, where both sulfur-bearing reaction

products are present in fluid conditions. On the other hand, the precipitation of elemental sulfur may precipitate directly from sulfate, and occur naturally in seawater occasionally at the beginning process of leaving sulfate marine aqueous medium. Youssef (1989) also studied the formation of elemental sulfur in Red Sea waters. He reported that some formulas may be applied to show how gypsum can be altered to carbonate and elemental sulfur. Through these reactions, it was postulated that there was an initial step of H_2S oxidation to form colloidal sulfur in the presence of excess SO_4^{2-} which lead to the concomitant alteration of gypsum in situ to dense calcite. Furthermore, the formed H_2S may react with Ca^{2+} and SO_4^{2-} to form calcium polysulfides in the water system. These polysulfides then react with CO_2 (produced by the oxidation of hydrocarbons) to cause the simultaneous precipitation of sulfur and calcite crystals. This suggested that sulfur was formed in a localized micro-environment in which the free interchange of sulfate with the surrounding environment was restricted. The precipitation of the epsomite ($MgSO_4 \cdot 7H_2O$) in the R.S. water was an indication of the excess of Mg^{2+} in an aqueous solution that follow the precipitation of aragonite (Fermani et al. 2017). This may be explained by the fact that Mg^{2+} absorbs into the calcite nuclei, thus preventing the integration of Ca^{2+} into the calcite crystal lattice, leading to the formation of the more compact aragonite crystal structure. This was apparent

Fig. 10 Sequential depositional model showing the order of evaporite salts, amounts, and types reference to water loss percentages during the isothermal evaporation of M.S. water

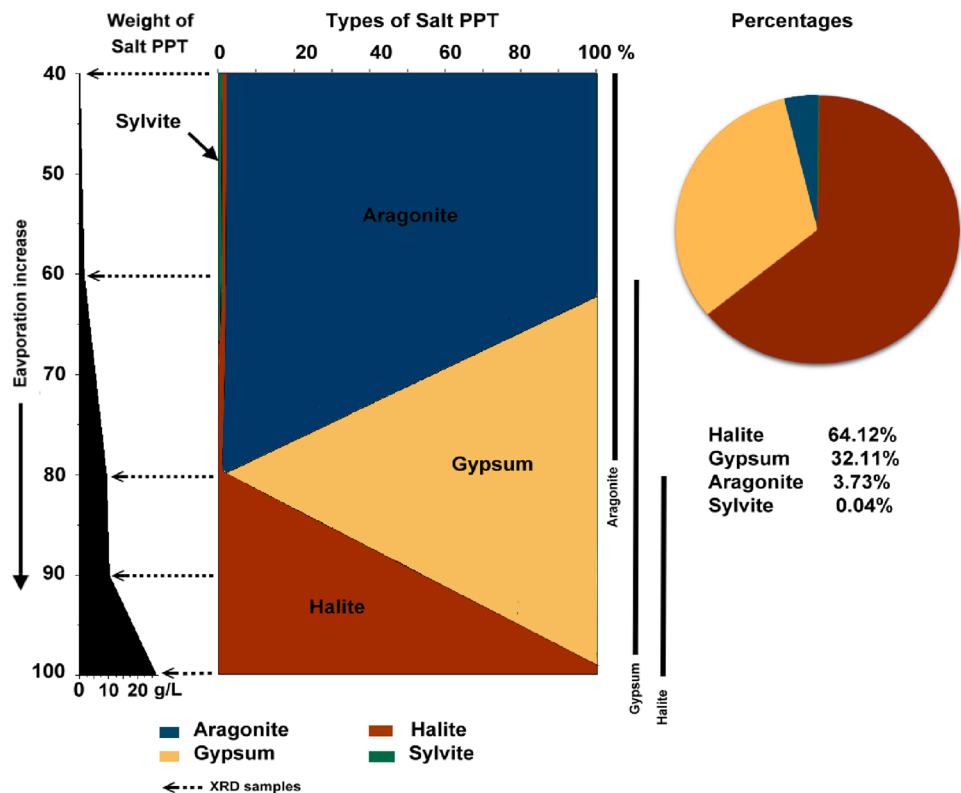
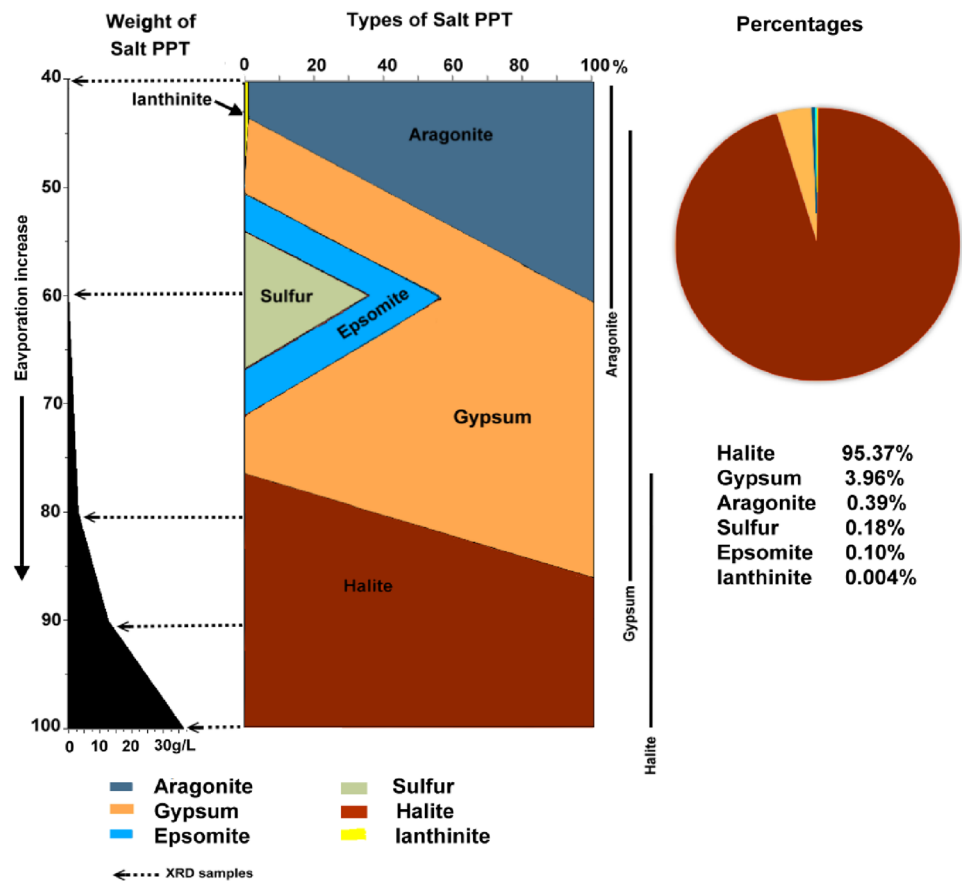


Fig. 11 Sequential depositional model showing the order of evaporite salts, amounts, and types reference to water loss percentages during the isothermal evaporation of R.S. water



in the case of R.S. water, in which epsomite was formed during the complete precipitation of aragonite.

At the 80% evaporation stage, evaporite precipitation was between 3.36 g/L (6.26%) and 9.32 g/L (19.48%) for the two respective seawaters. This stage represented the threshold precipitate of gypsum in the M.S. that reached 99% but with equal amounts of gypsum (52%) and halite (NaCl) (48%) for the R.S. water which may indicate gypsum threshold precipitate in the Red Sea that occurs at nearly 70% of the water loss (Figs. 6 and 7). As seen from these salts modeling Figs. 10 and 11, halite (NaCl) was the major end-product in the evaporite sequence that is characterized by being more soluble than the previous salts with the lowest density. The precipitation of halite was initiated with the depletion of gypsum deposits as the brine became richer in $MgSO_4$ and the chlorinity of water did increase. At this stage, the water chemistry may be characterized by $Ca \approx Mg$ and $HCO_3^- < Ca^{2+} + Mg^{2+}$ and salinity reaches 250‰ (Nichols 2022).

At the 90% and 100% water loss, the maximum accumulative amount of precipitated salts were (36.71 g/L; M.S.) represented by 76.72% and (49.85 g/L; R.S.) represented by 92.86%. These stages are the threshold accumulation of a considerably high amount of halite (NaCl) salt. While at 90% water loss of M.S., there is still an overlap between

depletion of gypsum (60%) and initiation of halite (40%) that transforms to complete halite precipitate during the next stage of absolute halite formed (Fig. 11).

From Figs. 10 and 11, it can be observed that the dominant salt in the case of the Mediterranean Sea was halite (64.12%). While in the case of the Red Sea, it comprises (95.37%) of the total salt precipitate. The second main dominant salt was gypsum comprised (32.11%; M.S.) and (3.96%; R.S.). Aragonite was the third main dominant salt with percentages of (3.73%; M.S.) and of (0.39%; R.S.). Other precipitate salts occur as an accessory to the total amount of a salt precipitate composed of sylvite (0.04%; M.S.), sulfur (0.18%; R.S.), epsomite (0.10%; R.S.), and ianthinite (0.004%; R.S.) (Figs. 10 and 11).

Volumetric models

The volume is a function of both mass (weight) and density characterizing each salt precipitate during the evaporation process. The volumetric model for evaporite salts precipitate in a geological sense mostly focuses on the ordering (sequence) and the vertical thickness of each deposited salt stratum. The present study volume models were illustrated to provide new prospects to the geologist whose interest in the salt industry concerning the quantity of deposited salts

and sequence of salts that precipitated out from both seawaters after complete evaporation. The densities of the main evaporite salts were 2.17 gm/cm³ (halite), 2.3 gm/cm³ (gypsum), 2.93 g/cm³ (aragonite), 2.06 g/cm³ (sulfur), 1.67 g/cm³ (epsomite), 1.99 g/cm³ (sylvite), and 5.16 g/cm³ (ianthinite) according to Nesse (2016) and Okrusch and Feimmel (2020).

Based on the salt densities and their percentages in bulk weight for the individual seawaters. The calculated average density of bulk salt deposited by evaporation of the M.S. water was approximately 2.23 g/cm³, representing an evaporite salt weight equal to 47.85 g/L, which represented a total volume of 21.43 cm³. For the R.S. water, the calculated bulk densities of bulk salt deposited were approximately 2.18 g/

cm³, representing an evaporate weight of 53.68 g/L which represented a total volume of 24.67 cm³.

The cubic root of volume in each case was visualized as the volumetric models of total evaporite salts, as shown in Fig. 12. From 2.78 cm as appears in a cross-section of evaporite salts deposited from 1000cm³ of M.S. water, volumetric models of salts as appearing in the cross-section are composed of halite (1.83 cm), gypsum (0.87 cm), aragonite (0.08 cm), and sylvite (0.0012 cm) (Fig. 12). While in the same case of volume models, of the R.S. water salts appear as 2.91 cm in cross-section composed of halite (2.86 cm), gypsum (0.11 cm), aragonite (0.01 cm), sulfur (0.006 cm), epsomite (0.004 cm), and ianthinite (0.00005 cm) in descending order (Fig. 12).

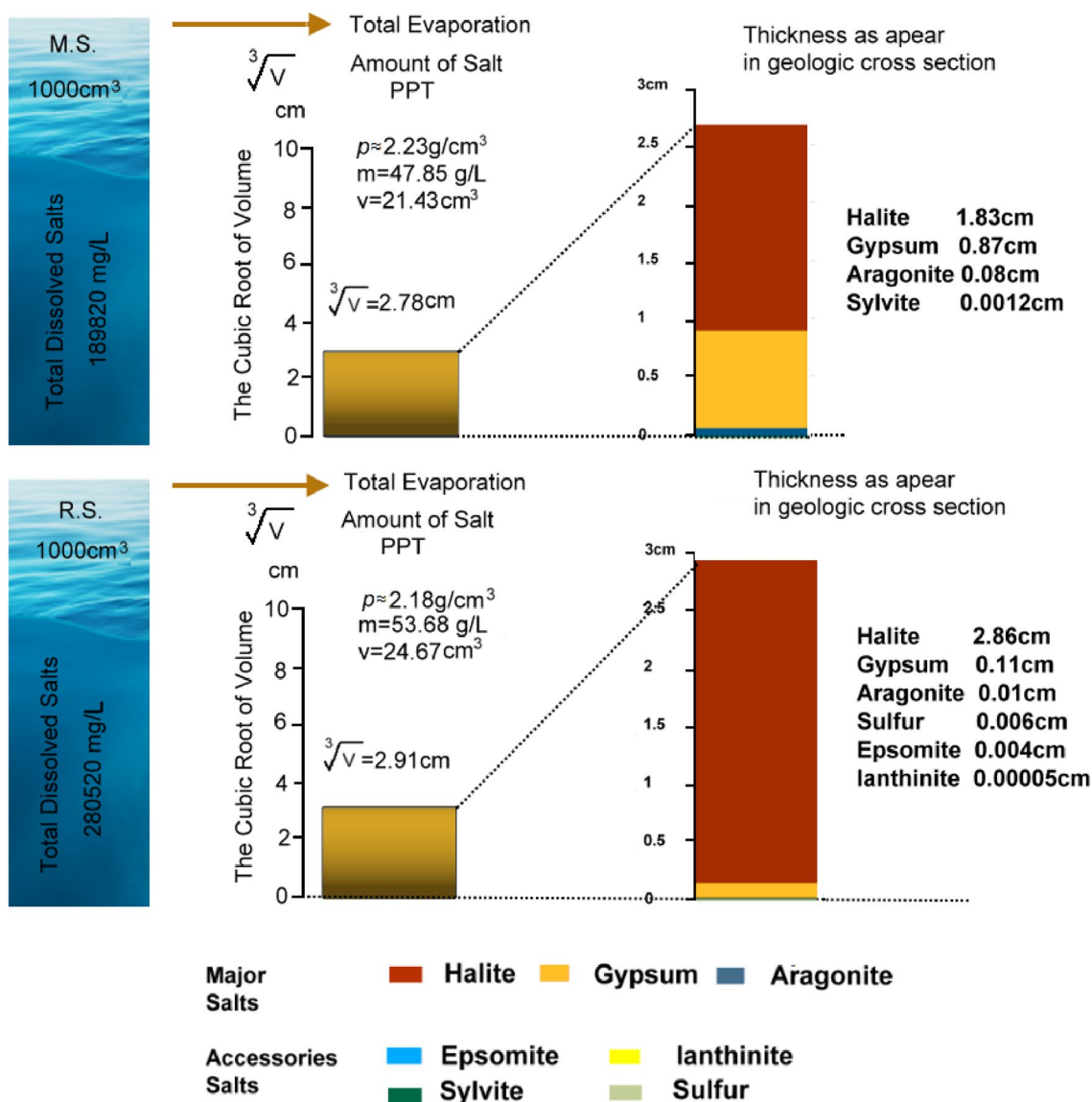


Fig. 12 Volumetric models of total gain evaporite salts from 1000cm³ (one liter) of seawaters as appear in vertical cross-section after complete evaporation of the M.S. and the R.S. waters

Applicability of the present study to understand the Messinian Salinity Crisis (MSC) and the Red Sea evaporite salts

Messinian and Red Sea evaporite basins are the youngest global Cenozoic–Mesozoic brine basins, ranging from 10 to 5 Ma (Evans 1990; Warren 2014). Messinian Salinity Crisis resulted in widespread salt precipitation due to the decrease in the Mediterranean Sea level equal to 1.5 km due to evaporation (Warny et al. 2003; Garcia-Castellanos and Villaseñor 2011; Karakitsios et al. 2017; Mousoulitotis et al. 2018). MSC was therefore responsible for the deposition of significant quantities of salts, representing the giant second evaporite basin throughout the earth's history. However, the chemistry and salinity of oceanic seawater, since 10 Ma has remained the same chemistry as the present-day oceans (Hay et al. 2006).

One of the important facts of the present study is that the amounts of salt precipitated from highly saline seawater were much higher than in the case of the same volume from less saline seawater (Fig. 12). This fact may be responsible for the increase in thickness of evaporite strata deposited from high salinity water relative to low salinity water sources during the same period. Generally, the threshold quantity of halite salts recorded was at 90–100% desiccation within the penesaline-B stage for brine development (Fig. 5).

Messinian evaporites that occupied the Red Sea and Mediterranean region during this period were estimated to result from salty water volume of 2,250,000 km³ for the Mediterranean basin and 900,000 km³ for the Red Sea basin (Ryan 2008). The north Nile Delta oil concession within Egypt recorded a so-called Rosetta Formation (Fm) that was composed of four evaporite cycles of anhydrite alternated by a streak of argillaceous limestone and mudstone reaching a maximum thickness of 408 m (Ismail et al. 2010; Farouk et al. 2014, 2021; Edress et al. 2022). The same equivalent of salt deposits was recorded within the Red sea region as the so-called Zeit Fm which was identified by anhydrite and halite with calcareous shale of a maximum thickness attain 515 m (Abd El Naby et al. 2017).

Based on the present study, the volume of evaporite deposited during the Messinian time was estimated to be 67,917,312 m³ relative to the 136,590,865 m³ attained from the modern-day Mediterranean Sea based on the conversion of thickness to volumetric amounts. The increase in evaporite volume and the presence of halite salts in the Red Sea (Zeit Fm) increased its salinity to the penesaline-B stage earlier than the Mediterranean Sea, which did not reach the penesaline-A stage during the MSC time (Fig. 5). This may be attributed to the dilution effect, as significant input from major river systems reached the Mediterranean basin compared with the Red Sea basin. Moreover, the presence of two additional older anhydrite evaporites formations in the Red

Sea basin, namely the Belayim Fm (237–280 m) consisting of anhydrite and calcareous shale and the South-Gharib Fm (219–581 m) consisting of salt (halite), anhydrite and calcareous shale of Late Serravallian-Tortonian (11.63 Ma) may indicate that the drying out of the Red Sea earlier than that of the Mediterranean Sea before the onset of the Messinian time (5.96–5.33 Ma) (Bosworth and McClay 2001; Evans 1990; Abd El Naby et al. 2017). Nevertheless, the present study estimation has appeared in a good sense in a general view. The Paleo evaporites' volumetric estimation thickness should be used restrictedly. Where the paleo-evaporites thickness, as recorded from the Red sea according to Smith and Santamarina (2022) exceeded ~1.5 times the present-day current thickness.

Conclusion

Depositional modeling of evaporite salts precipitated by evaporation of seawater of both R.S. and M.S. water was established in the present study based on the cooperation of analytical results of both water chemistry and types and quantity of salt precipitated isothermal hot climate conditions. The average rate of evaporation is measured statistically based on polynomial regression and linear correlation coefficient relationship between TDS and quantity of water evaporated per hour to be valid for further estimation of evaporation for any closed seawater body in any hot-arid regions. The major evaporite salts deposited from the present-day seawater of the M.S. and the R.S. are aragonite, gypsum, and halite in descending order where any other salts precipitate occurring as accessories. As the salinity of seawater increases as the end-product of halite salt increases in both the quantities and their volume appearance reach 95.37% in R.S of the saltiest seawater (salinity 34.5%) to 64.12% of fewer saltiest seawater (salinity 31%). The evaporation process led to the development of the brine from both seas, toward the formation of the MgSO₄ rich-seawater type. The present study modeling may help to estimate the amounts of gain salts or even the amount of water required for the production of a certain amount of salts for the geologist who is interested in the salt industry. Also, they give an idea of the time-consuming to accomplish of this process. Also, the volumetric models constructed from the present study may benefit in geological pastime in two ways: either to recognize the cumulative volume of salts required for a depositional of evaporite strata and/or to identify the stages of desiccation in the past related to the types of salt. In light of the present study, the volume of the evaporite salts deposited during the Messinian time in the Red Sea was twice the 136,590km³ that the evaporites volume deposited in the Mediterranean Sea (67,917km³) which may be attributed to

the increase in salinity of the Red Sea relative to the Mediterranean Sea waters at the Messinian time.

Supplementary Information The online version contains supplementary material available at <https://doi.org/10.1007/s40808-023-01698-2>.

Funding Not applicable.

Availability of data and materials Available based on the request of the journal.

Declarations

Conflict of interest The authors declare that there are no competing interests.

Ethics approval and consent to participate The authors declare that the content of the manuscript has not been published elsewhere.

Consent for publication All authors agree to consent for publication.

References

- Abd El Naby A, Abd-Elaziz W, Abdel Aal MH (2017) Biostratigraphy and seismic data analysis to detect the sequence stratigraphic depositional environment of the Miocene succession: Gulf of Suez (Egypt). *Swiss J Geosci* 110:777–791
- Babel M, Schreiber BC (2014) Geochemistry of Evaporites and Evolution of Seawater. In: Turekian K and Heinrich (eds) *Treatise on Geochemistry*, 2nd edn. Elsevier, Berlin, pp. 483–560.
- Borchardt-Ott W (2012) *Crystallography: An Introduction*. Springer Nature, Switzerland.
- Bosworth W, McClay K (2001) Structural and stratigraphic evolution of the Gulf of Suez rift, Egypt. In Ziegler PA, Cavazza, W, Robertson AHF, Crasquin-Soleau S (ed) *Peri-Tethys Memoir 6: Peri-Tethyan rift/wrench basins and passive margins*, Museum National d'Histoire naturelle de Paris, Memoirs, Paris pp. 567–606.
- Edress NAA, Fagelnour MS, Mahmoud AA (2022) Petrographic and organic geochemical studies of the Oligocene-Pliocene mud-rich formations East Mediterranean concession Egypt. *Arab J Geosci*. <https://doi.org/10.1007/s12517-022-10742-x>
- Einsele G (2000) *Sedimentary basins: evolution, facies, and sediment budget*. Springer
- Elhossainy MM, Albaroot M, Al-Areeq NM, Salman AM (2022) Late Jurassic Safir evaporite salts, Sab'atayn Basin, Yemen: lithofacies distribution, cyclicality, and mineralogy. *J Afr Earth Sc* 195:104641
- Engineering ToolBox (2004) *Evaporation from Water Surface*. https://www.engineeringtoolbox.com/evaporation-water-surface-d_690.html
- Evans AL (1990) Miocene sandstone provenance relationships in the Gulf of Suez: insights into syn-rift unroofing and uplift history. *Am Assoc Petroleum Geologists* 74:1386–1400
- Farouk S, Ziko A, Eweda SA, Said AE (2014) Subsurface Miocene sequence stratigraphic framework in the Nile Delta, Egypt. *J Afr Earth Sci* 91:89–109
- Farouk S, Jain S, Abd-Elaziz M, El Shennawy T, Shaker F (2021) High-resolution Pliocene-Pleistocene calcareous nannofossil distribution and palaeoenvironmental changes in the northwest Nile Delta, Egypt. *Lethaia* 54:845–870
- Fermani S, Njegić Džakula B, Reggi M, Falini G, Kralj D (2017) Effects of magnesium and temperature control on aragonite crystal aggregation and morphology. *Cryst Eng Comm* 19:2451–2455
- Garcia-Castellanos D, Villaseñor A (2011) Messinian Salinity Crisis regulated by competing tectonics and erosion at the Gibraltar arc. *Nature* 480(7377):359–363. <https://doi.org/10.1038/nature10651>
- Garrett DE (1996) Origin of potash deposits. In: Potash, Chapman and Hall (ed). Springer, Dordrecht, pp 1–80.
- Hardie LA (1991) On the significance of evaporites. *Ann Rev Earth Planetary Sci* 19:131–168
- Hay WH, Migdisov A, Balukhovskiy AN, Wold CN, Fogel S, Soding E (2006) Evaporites and the salinity of the ocean during the Phanerozoic: implications for climate, ocean circulation and life. *Palaeogeogr Palaeoclimatol Palaeoecol* 240:3–46
- Hazen RM, Ewing RC, Sverjensky DA (2009) Evolution of uranium and thorium minerals. *Am Miner* 94:1293–1311
- Hovorka SD (1992) Halite pseudomorphs after gypsum in bedded anhydrite-clue to gypsum-anhydrite relationships. *J Sediment Petrol* 62(6):1098–1111
- Ismail AA, Boukhary M, Naby A (2010) Subsurface stratigraphy and micropaleontology of the Neogene rocks, Nile Delta, Egypt. *Geol Croat* 63(1):1–26. <https://doi.org/10.4154/GC.2010.01>
- Karakitsios V, Cornée J, Tsourou T, Moissette P, Kontakiotis G, Agiadi K, Manoutsoglou E, Triantaphyllou M, Koskeridou E, Drinia H, Roussos D (2017) Messinian Salinity Crisis record under strong freshwater input in marginal, intermediate, and deep environments: The case of the North Aegean. *Palaeogeogr Palaeoclimatol Palaeoecol* 485:316–335
- Khalil M, Elharairy M, Atta E et al (2021) Evaluation of salts in salt pans, Siwa Oasis, Egypt. *Arab J Geosci* 14:770. <https://doi.org/10.1007/s12517-021-07060-z>
- Leeder M (2011) *Sedimentology and sedimentary basins: from turbulence to tectonics*. Blackwell Publishing
- Mousouliotis A, Albanakis K, Georgakopoulos A (2018) Messinian clastic deposition and Halokinesis over the Premessinian geomorphology, Herodotus Basin, Eastern Mediterranean. Eastern Mediterranean Workshop, European Association of Geoscientists & Engineers, <https://doi.org/10.3997/2214-4609.201803041>
- Nash DJ, McLaren SJ (2011) *Geochemical sediments and landscapes*. Wiley-Blackwell
- Nesse WD (2016) *Introduction to mineralogy*. Oxford University Press
- Nichols G (2022) *Sedimentology and stratigraphy*. Wiley-Blackwell Publishing
- Okrusch M, Feimmel HE (2020) *Mineralogy: an introduction to minerals, rocks, and mineral deposits*, Springer textbooks in earth sciences geography and environment. Springer, p 1971
- Ostad-Ali-Askari K, Shayannejad M, Eslamian S (2017) Deficit irrigation: optimization models. Management of drought and water scarcity. In: *Handbook of drought and water scarcity*, Taylor & Francis Publisher, United Kingdom, pp: 373–389
- Robert CM (2009) *Global sedimentology of the ocean: an interplay between geodynamics and paleoenvironment*. Elsevier
- Ryan WBF (2008) Modeling the magnitude and timing of evaporative drawdown during the Messinian Salinity Crisis. *Stratigraphy* 5:227–243
- Singh Y, Viswanathan R, Parashar KK, Srivastava SK, Ramesh-Babu PV, Parihar PS (2014) Ianthinite: a rare hydrous uranium oxide mineral from Akkavaram, Andhra Pradesh, India. *J Earth Syst Sci* 123(1):15–19
- Smith JE, Santamarina JC (2022) Red sea evaporites: formation, creep and dissolution. *Earth Sci Rev* 232:104115
- Sonnenfeld P (1989) Genesis of evaporites. Part. I. In: Sonnenfeld P. y Perthuisot J.P., Brines and evaporites. 28th International Geological Congress, Short Course in Geology (Crawford M.L. y Padovani E., Short Course Series Editors.). American Geophysical Union, 3:1–128
- Talebmorad H, Ahmadnejad A, Eslamian S, Ostad-Ali-Askari K (2020) Evaluation of uncertainty in evapotranspiration values by FAO56-Penman-Monteith & Hargreaves-Samani methods. *Int J Hydrol*

- Sci Technol 10(2):135–147. <https://doi.org/10.1504/IJHST.2020.106481>
- Talebmorad H, Abedi-Koupai J, Eslamian S, Mousavi S, Akhavan S, Ostad-Ali-AskariSingh KVP (2021) Evaluation of the impact of climate change on reference crop evapotranspiration in Hamedan-Bahar plain. *Int J Hydrol Sci Technol* 11(3):333–347. <https://doi.org/10.1504/IJHST.2021.114554>
- Tucker ME (2001) *Sedimentary petrology*. Blackwell Science, Oxford
- Tucker ME, Jones SJ (2022) *Sedimentary petrology*, 4th edn. Wiley-Blackwell Publishing
- Warny SA, Bart PJ, Suc JP (2003) Timing and progression of climatic, tectonic and glacioeustatic influences on the Messinian Salinity Crisis. *Palaeogeogr Palaeoclimatol Palaeoecol* 202:59–66
- Warren JK (2008) Salt as sediment in the Central European Basin system as seen from a deep time perspective. In: Littke R (ed) *Dynamics of complex intra-continental basins: The Central European Basin System*. Springer-Verlag, Berlin, pp 249–276
- Warren JK (2014) Geochemistry of evaporite ores in an earth-scale climatic and tectonic framework. In: Holland HD, Turekian KK (eds) *Treatise on geochemistry*, 2nd edn. Elsevier, Oxford, pp 569–593
- Warren JK (2021) Evaporite deposits. In: Alderton D, Elias SA (eds) *Encyclopedia of geology*, 2nd edn. Academic Press, Oxford, pp 945–977
- Youssef EAA (1989) Geology and genesis of sulfur deposits at Ras Gamsa area Red Sea coast, Egypt. *Geology* 17(9):797801. [https://doi.org/10.1130/0091-7613\(1989\)017%3c0797:GAGOSD%3e2.3.CO;2](https://doi.org/10.1130/0091-7613(1989)017%3c0797:GAGOSD%3e2.3.CO;2)
- Zhong S, Mucci A (1989) Calcite and aragonite precipitation from seawater solutions of various salinities: Precipitation rates and overgrowth compositions In: Schott J and Lasaga AC (eds) *Kinetic Geochemistry Chem. Geol.* pp 283–299

Publisher's Note Springer Nature remains neutral with regard to jurisdictional claims in published maps and institutional affiliations.

Springer Nature or its licensor (e.g. a society or other partner) holds exclusive rights to this article under a publishing agreement with the author(s) or other rightsholder(s); author self-archiving of the accepted manuscript version of this article is solely governed by the terms of such publishing agreement and applicable law.